2018

Transient Simulation of Small-Capacity Reciprocating Compressors for On-Off Controlled Refrigerators

Marco C. Diniz
POLO / UFSC, Brazil, marcodiniz@polo.ufsc.br

Christian Hermes
POLO Labs, Federal University of Santa Catarina, Brazil, hermes@polo.ufsc.br

Marco C. Diniz
deschamps@polo.ufsc.br

Transient Simulation of Small-Capacity Reciprocating Compressors for On-Off Controlled Refrigerators

Marco C. DINIZ, Christian J. L. HERMES, Cesar J. DESCHAMPS [*]

POLO Research Laboratories for Emerging Technologies in Cooling and Thermophysics
Department of Mechanical Engineering, Federal University of Santa Catarina
88040900 Florianopolis, SC, Brazil

[*]Corresponding Author: deschamps@polo.ufsc.br

ABSTRACT

This paper presents a simulation model for the transient behavior of vapor compression refrigerating appliances subjected to on-off control patterns focusing on the reciprocating compressor. A detailed compressor model is put forward based on two sub-models: one for the compression cycle, which can predict the valve dynamics, heat transfer in the compression chamber and the pressure pulsations in mufflers, and the other for the compressor shell, which calculates the temperature and mass flow rate in components other than the compression chamber. The remaining components of the single-door frost-free refrigerator considered in this work (i.e. condenser, evaporator, refrigerated compartment) are modeled based on mass and energy balances considering each component as an even lump. The expansion device and the refrigerant charge sub-models are replaced by prescribed condenser subcooling and evaporator superheating degrees, respectively. The overall cycle simulation model was validated by comparing predictions for the compressor temperatures and mass flow rate, indicated power, power consumption and overall energy consumption with the experimental counterparts measured in a household refrigerator, whose components – including the compressor – were carefully instrumented with thermocouples and pressure transducers, and tested in a climate chamber with a strict control of air temperature, humidity and velocity. Finally, sensitivity analyses were conducted to compare the effect of the compressor design parameters on its performance under calorimeter and actual system conditions.

1. INTRODUCTION

About 1.4 billion household refrigerators and freezers are in use (Barther and Götz, 2012), i.e. roughly one refrigerator for each five inhabitants of the globe. Since such appliances are responsible for consuming around 15% of the electrical energy produced for the residential sector, governments worldwide are increasingly launching more stringent energy policies, promoting a continuous development of refrigerating devices (Belman-Flores *et al.*, 2015).

Virtually any refrigerators available on the market employ vapor compression refrigeration cycles with reciprocating compressors. Since the cooling capacity of the system is usually higher than the thermal loads, a strategy to maintain the temperatures in the compartments at the desired levels is required. The most common and less costly method consists of matching the cooling capacity to the thermal loads by means of a thermostat which switches the compressor on and off. The periodic compressor start-up and shut-down gives rise to transient phenomena such as pressure peaks and equalization, refrigerant migration and evaporator activation, with the working pressures and mass flow rates spanning a wide range of operating conditions which can be quite different from the steady-state ones usually considered for component matching and compressor design (Hermes and Melo, 2008).

For a better understanding of the effect of the transient (start-up/shut-down) operating conditions upon the compressor performance, a system simulation model is required. On the one hand, the models developed for vapor compression cycles under on-off conditions are frequently focused on the heat exchangers and the refrigerated compartments (Borges *et al.*, 2015; Heimel *et al.*, 2016), while simplified modeling approaches are commonly adopted for the compressor, which are based on maps of volumetric and overall efficiencies to estimate mass flow rate and power consumption (Ndiaye and Bernier, 2010; Negrao *et al.*, 2011). Just a few works, such as the ones published by Chen and Lin (1991) and Hermes and Melo (2008), presented more elaborate models for the compression cycle, albeit neglecting key aspects of the compressor performance such as valve dynamics and pressure pulsations in the suction

and discharge mufflers. On the other hand, these phenomena are taken into account in some compressor models available in the literature, such as the one presented by Todescat *et al.* (1992), which depend on external boundary conditions for the working pressures (evaporating, condensing) and suction line temperature, supplied to the model in an open-loop, thus transmitting information from the system to the compressor, but not the other way round.

To the best of our knowledge, there is no study in the open literature focusing on the compressor behavior due to the transient phenomena imposed to the refrigeration cycle by the on-off control patterns. Therefore, this work is aimed at advancing a cycle simulation model which is able not only to predict on-off cycling transients but also the detailed heat and fluid flow dynamics inside the compressor. A single-door frost-free refrigerator designed for the Brazilian market was adopted in this study. The refrigerant flow through the heat exchangers and the expansion device was modeled following a quasi-steady-state approach, where the heat exchangers (condenser, evaporator) and the refrigerated compartments have each been simulated as even lumps. A detailed model was implemented for the compressor, being comprised of two sub-models – namely, one for the compression cycle and the other for the heat transfer in the compressor shell. The key parameters required by the model were derived from measurements, which were also used to validate the model predictions in different operating conditions.

2. MATHEMATICAL MODELING

2.1 Compressor

The compressor model follows the procedure described by Diniz *et al.* (2016), according to which a transient compression cycle sub-model and a thermal compressor shell sub-model, that calculates the temperatures in other compressor components, are solved in a coupled manner. The model for the compression cycle is based in four groups of equations, as described by Todescat *et al.* (1992). The first one allows the calculation of the instantaneous volume occupied by the gas inside the compression chamber, $\forall_g^i$,

$$\forall_g^i(\theta) = \frac{\pi D_{cc}^2}{4}\left(d_{TDC} - \left\{e\cos\theta + [L_r^2 - (e\sin\theta - d_m)^2]^{1/2}\right\}\right) + \forall_c \tag{1}$$

where $\forall_c$ is the dead volume and D_{cc}, d_{TDC}, e, L_r and d_m are geometric parameters, as depicted in Fig. 1. The second group of equations is obtained by applying the conservation equations to the compression chamber, as illustrated in Fig. 2. The resulting mass conservation equation is expressed as follows,

$$\frac{dm_g^i}{dt} = \dot{m}_{suc}^i - \dot{m}_{dis}^i - \dot{m}_l^i - \dot{m}_{b,suc}^i + \dot{m}_{b,dis}^i \tag{2}$$

where $\dot{m}_{suc}^i$ and $\dot{m}_{dis}^i$ are the instantaneous mass flow rates through the suction and discharge valves, with the subscript b representing backflow in both valves, and $\dot{m}_l^i$ is the instantaneous leakage through the piston-cylinder clearance. With the instantaneous mass and volume of refrigerant inside the compression chamber it is possible to estimate its density. The instantaneous temperature of the refrigerant inside the compression chamber is obtained by means of the energy conservation equation,

$$\frac{dT_g^i}{dt} = A - BT_g^i \tag{3}$$

$$A = \frac{1}{m_g^i c_v^i}\left[\hbar_w A_w^i T_w - h_g^i \frac{dm_g^i}{dt} + (\dot{m}_{suc}^i h_{sc}) - (\dot{m}_{dis}^i h_g^i) - (\dot{m}_l^i h_g^i) - (\dot{m}_{b,suc}^i h_g^i) + (\dot{m}_{b,dis}^i h_{dc})\right] \tag{4}$$

$$B = \frac{1}{m_g^i c_v^i}\left[\hbar_w A_w^i + \frac{\partial p_g}{\partial T_g}\bigg|_v \frac{d\forall_g^i}{dt} - \frac{\partial p_g}{\partial T_g}\bigg|_v v_g^i \frac{dm_g^i}{dt}\right] \tag{5}$$

where $\hbar_w$, is the convective heat transfer coefficient (Annand, 1963). The temperatures of the suction chamber (T_{sc}), discharge chamber (T_{dc}) and cylinder wall (T_w) are predicted by the thermal model. With the temperature calculated from Equation (3) and the density of the refrigerant it is possible to estimate the pressure inside the compression chamber using an equation-of-state (in the p-v-T form) for the refrigerant under analysis.
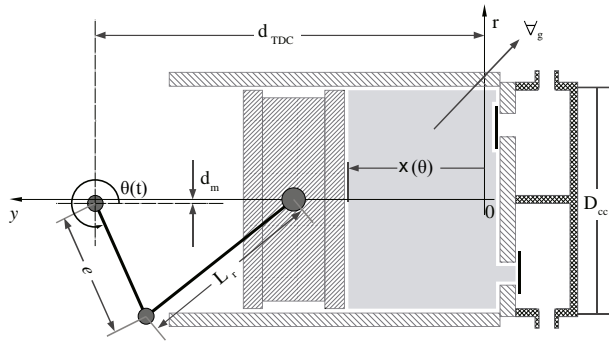
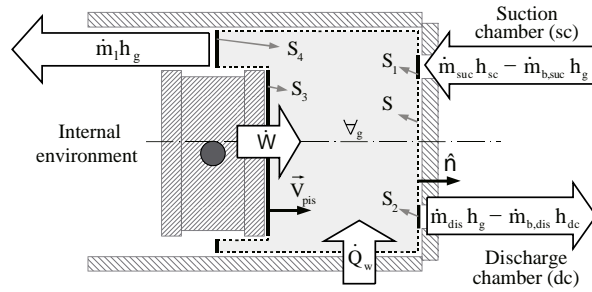**Figure 1:** Schematic representation of the compression chamber

Figure 2: Mass and energy fluxes within the compression chamber

The third group of equations is required to calculate valve dynamics. A single degree-of-freedom mass-spring model is employed, with effective force areas being used to characterize the flow-induced force acting on the valve. Finally, the fourth group of equations predicts the mass flow rates that cross the control volume surface depicted in Fig. 2. The mass flow rates through the valves are estimated using the effective flow area to correct the theoretical value given by the relation for isentropic flow through convergent nozzle. Refrigerant leakage through the clearance between piston and cylinder is estimated by considering a fully developed laminar Couette-Poiseuille flow (Ferreira and Lilie, 1984). In this work, pressure pulsations in the suction and discharge mufflers are calculated with the model presented by Deschamps *et al.* (2002).

Since the time scale of the compression cycle (milliseconds) is considerably smaller than that of the compressor shell transients (minutes), the outputs from the compression cycle model must be averaged over a representative cycle, using the relations shown in Table 1. The mechanical losses $\dot{Q}_b$ and the electrical efficiency η_{ele} were specified based on experimental data previously obtained for the compressor under analysis, while the average heat dissipation due to friction in the piston-cylinder gap, $\dot{Q}_{pc}$, is calculated according to Ferreira and Lilie (1984).

Table 1: Output from the compression chamber model.

Parameter	Calculation
$\dot{W}_{ind}$	$-f \oint p_g d\forall_g$
$\dot{m}_{suc}, \dot{m}_{dis}, \dot{m}_l, \dot{m}_{b,suc}$ and $\dot{m}_{b,dis}$	$\frac{1}{2\pi} \int_0^{2\pi} \dot{m}_k^i \, d\theta$, where $k = suc, k = dis, k = l, k = b, suc$ or $k = b, dis$
$\dot{Q}_{pc}$	$\frac{1}{2\pi} \int_0^{2\pi} \dot{Q}_{pc}^i \, d\theta$
$\dot{Q}_{mot}$	$(\dot{W}_{ind} + \dot{Q}_{pc} + \dot{Q}_b)/\eta_{ele} - (\dot{W}_{ind} + \dot{Q}_{pc} + \dot{Q}_b)$

The compressor thermal model follows an integral approach, in which the compressor is divided into several non-overlapping control volumes, as illustrated in Figure 3, where mass and energy balances are applied. The energy balances have the following general form (Diniz *et al.*, 2016):

$$\frac{d}{dt}(mu) = \sum \dot{m}h|_{in} - \sum \dot{m}h|_{out} + \dot{Q} - \dot{W} \qquad (6)$$

The thermal conductances were estimated by adjusting the model to a known (measured) steady-state temperature distribution, as suggested by Todescat *et al.* (1992). The transient terms in the system of equations were not considered in this procedure. The condition chosen for the model adjustment is represented by the evaporating temperature $T_e = -25.8$ °C, condensing temperature $T_c = 44.6$ °C, suction line temperature $T_{sl} = 28.6$ °C and ambient temperature $T_{amb} = 32$ °C. The adjusted heat conductances were held constant throughout the transient simulation exercise.
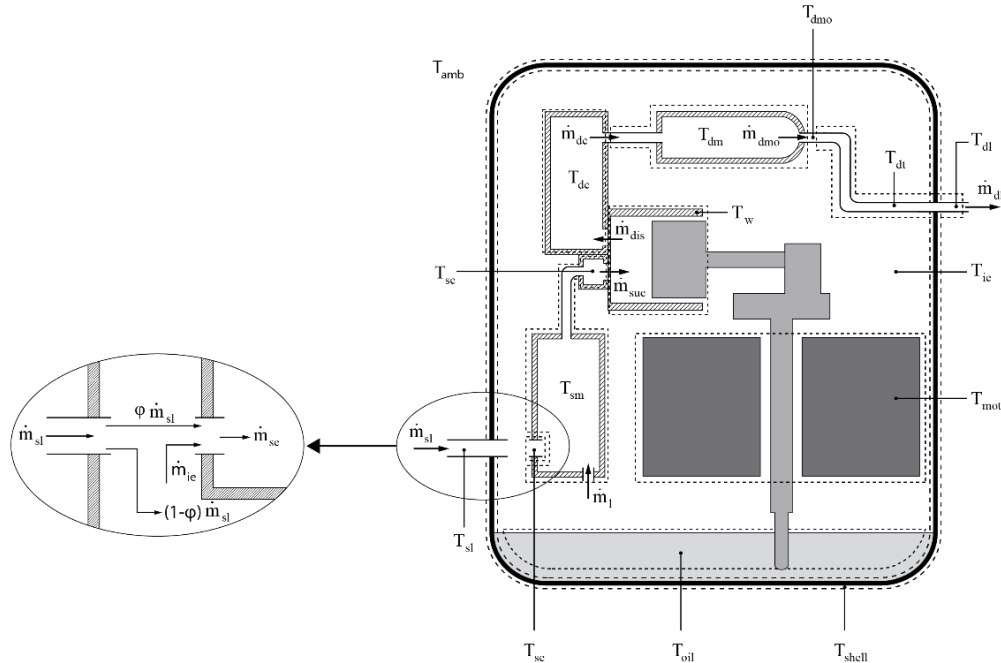
Figure 3: Schematic of the compressor shell model and the control volumes used for the thermal analysis

2.2 Condenser and evaporator

A lumped quasi-steady-state approach (Borges *et al.*, 2010) was adopted to simulate the refrigerant flow in the evaporator and the condenser, where the thermal inertia of the condenser and evaporator walls were also incorporated into the model (Tagliafico *et al.*, 2012; Borges *et al.*, 2015). The energy balances in the condenser yield

$$UA_{c-cd}(T_c - T_{cd}) = \dot{m}(h_{dl} - h_{cd,out}) \tag{7}$$

$$C_{cd}\left(\frac{T_{cd}^t - T_{cd}^{t-\Delta t}}{\Delta t}\right) = UA_{c-cd}(T_c - T_{cd}) - UA_{cd-amb}(T_{cd} - T_{amb}) \tag{8}$$

where T_{amb} is the surrounding air temperature, T_c is the condensing temperature, T_{cd} is the condenser wall temperature, $\dot{m}$ is the mass flow rate discharged by the compressor, C_{cd} is the thermal capacity of the condenser wall, UA_{c-cd} and UA_{cd-amb} are, respectively, the thermal conductances between the refrigerant and the wall, and between the condenser wall and the surrounding air, and h_{dl} is the specific enthalpy of the refrigerant at the compressor discharge. The specific enthalpy at the condenser outlet is $h_{cd,out} = h(p_c, T_c - \Delta T_{sub})$, where ΔT_{sub} is the subcooling degree imposed to the condenser outlet in replacement of the expansion device model (Borges *et al.*, 2010). The energy balances in the evaporator yield

$$UA_{ev-e}(T_{ev} - T_e) = \dot{m}(h_{ev,out} - h_{ev,in}) \tag{9}$$

$$C_{ev}\left(\frac{T_{ev}^t - T_{ev}^{t-\Delta t}}{\Delta t}\right) = UA_{rc-ev}(T_{rc} - T_{ev}) - UA_{ev-e}(T_{ev} - T_e) \tag{10}$$

where T_{rc} is the temperature of the refrigerated compartment, T_e is the evaporating temperature, T_{ev} is the evaporator wall temperature, C_{ev} is the thermal capacity of the evaporator wall, UA_{ev-e} and UA_{rc-ev} are, respectively, the thermal conductances between the evaporator wall and the refrigerant, and between the refrigerated compartment and the evaporator wall, and $h_{ev,in}$ is the specific enthalpy of the refrigerant at the evaporator inlet, calculated from the internal heat exchanger model. The specific enthalpy at the evaporator outlet is $h_{ev,out} = h(p_e, T_e + \Delta T_{sup})$, where ΔT_{sup} is the superheating degree imposed to the evaporator outlet in replacement of the refrigerant charge model (Borges *et al.*, 2010).

2.3 Internal heat exchanger

In the cases where an internal heat exchanger between the capillary tube and the suction line is employed, the expansion process in capillary tube takes place while rejecting heat to the suction line, yielding

$$h_{sl} = h_{ev,out} + \varepsilon c_{p,v}\left(T_{cd,out} - T_{ev,out}\right) \tag{11}$$

$$h_{ev,in} = h_{cd,out} + \varepsilon c_{p,v}\left(T_{cd,out} - T_{ev,out}\right) \tag{12}$$

where ε is the effectiveness of the internal heat exchanger, whereas h_{sl} is the refrigerant enthalpy at the compressor suction, $T_{cd,out}$ and $T_{ev,out}$ are the temperatures at the condenser and the evaporator outlets, respectively, and $c_{p,v}$ is the specific heat of saturated vapor at the evaporating pressure.

2.4 Refrigerated compartment

The refrigerated compartment is modeled according to the following energy balance,

$$C_{rc}\left(\frac{T_{rc}^t - T_{rc}^{t-\Delta t}}{\Delta t}\right) = UA_{amb-rc}(T_{amb} - T_{rc}) - UA_{rc-ev}(T_{rc} - T_{ev}) + \dot{W}_{fan} \tag{13}$$

where C_{rc} is the thermal capacity of the refrigerated compartment, UA_{amb-rc} is the thermal conductance between the surrounding air and the refrigerated compartment, and $\dot{W}_{fan}$ is the power dissipation in the fan.

2.5 Solution procedure

The model can be initialized in a condition at which the compressor is switched off. In this case, initial temperatures must be prescribed for the all the control volumes that employ transient models. Such temperatures can be obtained from a prior steady-state simulation. When the compressor is off, only the compressor thermal model, the evaporator wall model, the condenser wall model and the model for the refrigerated compartment are solved. The temperature of the refrigerated compartment increases until it reaches the thermostat start-up temperature, when the compressor is switched on, so that the compression cycle model and the quasi-steady models for refrigerant flow through the heat exchangers are also activated. Since exchange of data between the sub-models for the components of the refrigeration cycle is necessary, an iterative numerical procedure at each time step is adopted through the Newton-Raphson algorithm. Convergence at each time step is verified using a criterion based on the compressor discharge temperature. The calculation takes place until the thermostat cut-off temperature is reached. This procedure is repeated for many on-off cycles so that a periodic-steady-state condition is achieved. The model was coded in C++, whereas the refrigerant properties were calculated from *Refprop* database (Lemmon *et al.*, 2002).

3. EXPERIMENTAL PROCEDURE

The system under analysis is a single-door 300-L frost-free refrigerator running with R600a, which was carefully instrumented to obtain the electrical power consumption, pressure in the compressor inlet and outlet ports and mass flow rate at the compressor discharge line, as depicted in Fig. 4. T-type thermocouples were adopted to measure the temperatures at the inlet and outlet of each of the cycle components, and the temperature of the refrigerated compartment were also monitored and recorded. The reciprocating compressor provides 5.96 cm³/rev at 50 Hz and employs ISO-5 alkylbenzene as the lubricant oil. The compressor was instrumented to obtain the temperatures in several locations following the refrigerant path, besides solid components and lubricant oil, as shown in Fig. 5. A piezo-electric pressure transducer was installed to measure the pressure inside the compression chamber during the compression cycle. Details about the instrumentation and the experimental procedure can be found in Diniz *et al.* (2018). The tests were carried out in a climate chamber capable of maintaining the air temperature, humidity and velocity under strictly controlled conditions. Three ambient temperatures (T_{amb} = 32 °C, 25 °C and 16 °C) and three thermostat cut-off temperatures (T_{off} = -19 °C, -16 °C and -10 °C) were combined to generate 9 different test conditions. Measurements of a typical on-period under a test condition with T_{amb} = 32 °C and T_{off} = -16 °C were used to derive the semi-empirical parameters of the model: UA_{c-cd} = 32.0 W/K, UA_{cd-amb} = 8.8 W/K, UA_{rc-ev} = 11.0 W/K, UA_{ev-e}=52.0 W/K, UA_{amb-rc} = 1.25 W/K, C_{rc} = 10830 J/kg and ε = 0.81).
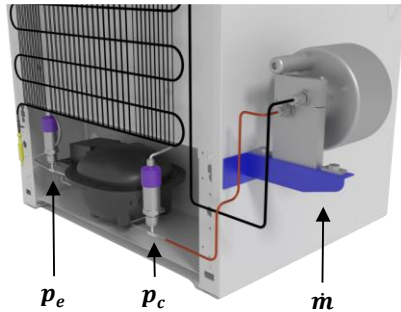
Figure 4: Schematic of the compressor compartment with pressure and mass flow rate instrumentation
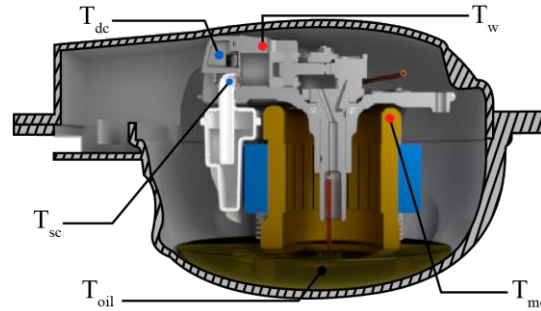

Figure 5: Schematic of the compressor instrumentation with T-type thermocouples

4. RESULTS AND DISCUSSION

Fig. 6 shows the experimental results for evaporating pressure, p_e, condensing pressure, p_c, and compressor suction line temperature, T_{sl}, during the on-period when the refrigerator is operating at $T_{amb} = 32$ °C and $T_{off} = -16$ °C. In order to evaluate the accuracy of the compressor simulation separately from the system, the experimental data plot in Fig. 6 were inputted to the compressor model alone. The results of this assessment are shown in Figs. 7 to 9. Fig. 7 compares the model predictions for the indicated power, $\dot{W}_{ind}$, electrical power, $\dot{W}_{ele}$ and mass flow rate, $\dot{m}_{dl}$, with their experimental counterparts, with an agreement within 2% being observed for the whole on-period. Figures 8 and 9 show, respectively, the pressure-volume diagram 30 s after the compressor start-up and just before the shut-down. Again, good agreement is seen between predictions and measurements.
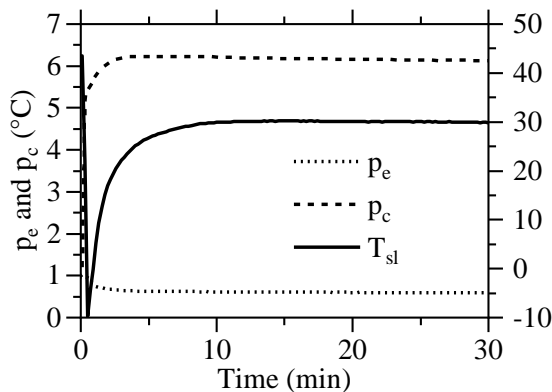

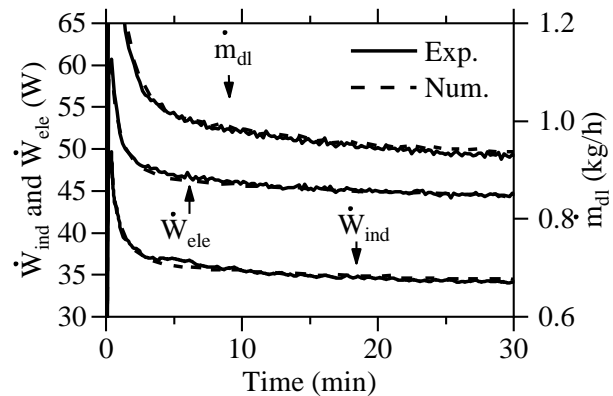**Figure 6:** Experimental results of the variables inputted to the compressor model alone

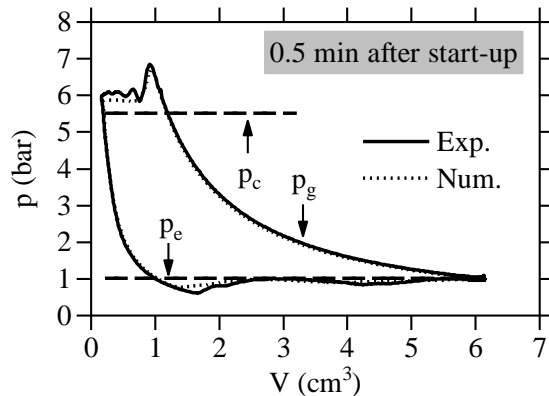**Figure 7:** Numerical vs. experimental results of power consumption and mass flow rate

Figure 8: Comparison between measured and predicted $p - \forall$ diagrams after compressor start-up
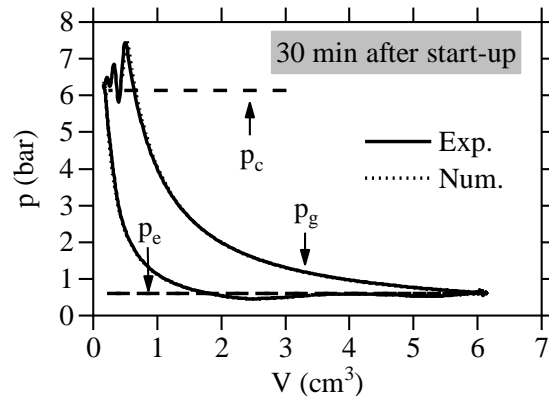

Figure 9: Comparison between measured and predicted $p - \forall$ diagrams before compressor shutdown

After being validated, the compressor model was used together with the system simulation model to evaluate the transient phenomena causing the thermodynamic losses and reducing the mass flow rate. Figures 10 to 13 compare experimental measurements with model predictions during the on-period when the system is operating at $T_{amb} = 32$ °C and $T_{off} = -16$ °C. Fig. 10 shows the time evolution of the evaporating temperature, T_e, condensing temperature, T_c, and temperature of the refrigerated compartment, T_{rc}, with good agreement between numerical and experimental results, especially after 5 minutes on, with deviations lower than 2 °C. One can see that during the first few minutes of the on-period, the model predicts an evaporating temperature significantly lower than the experimental counterpart, which is explained by the quasi-steady approach that does not consider the advance of the two-phase boundary inside the evaporator coil and the refrigerant mixture with oil during the off period. As a consequence, the model underestimates mass flow rate and power consumption during the first few minutes of the on-period, as can be seen in Fig. 11, which compares predictions for $\dot{W}_{ind}$, $\dot{W}_{ele}$, and $\dot{m}_{dl}$, with the experimental counterparts. After 5 minutes on, the model is able to predict the power consumption and mass flow rate with differences around 1% and 3%, respectively, which are within the experimental uncertainty.
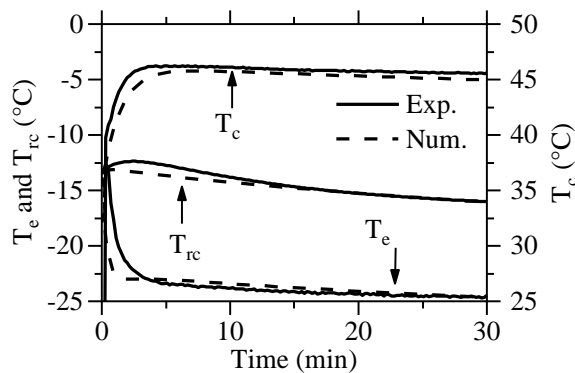

Figure 10: Numerical vs. experimental results of the variables inputted to the compressor model
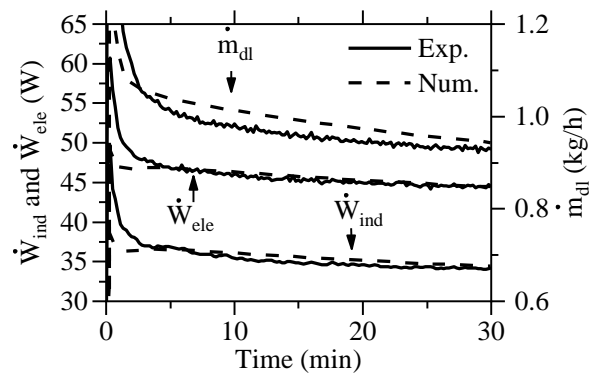

Figure 11: Numerical vs. experimental results of power consumption and mass flow rate

Fig. 12 shows the temperatures along the refrigerant path inside the compressor, such as suction line, suction chamber, discharge chamber and discharge line. One can see that the model is not able to predict the suction line temperature, T_{sl}, just after compressor start-up, partially due to the simplifications adopted for the condenser and evaporator model, particularly the fixed degrees of subcooling and superheating in the condenser and evaporator exits, respectively. A moving-boundary formulation for the evaporator would certainly bring about better results. Despite the deviations observed in Fig. 12 for the early stages, the differences between the experimental and numerical results were typically around 2 °C for most of the time. Fig. 13 shows the temperatures of the internal components (electric motor, compressor shell and cylinder wall temperature) and lubricant oil. Good agreement is seen between the experimental and numerical counterparts throughout the on-period, except for the oil, for which a constant heat conductance throughout the transient simulation is not appropriate. It is also interesting to observe that the cylinder wall temperature presents the highest amplitude of variation during the on-period, while motor temperature is practically stable due to its high thermal inertia.
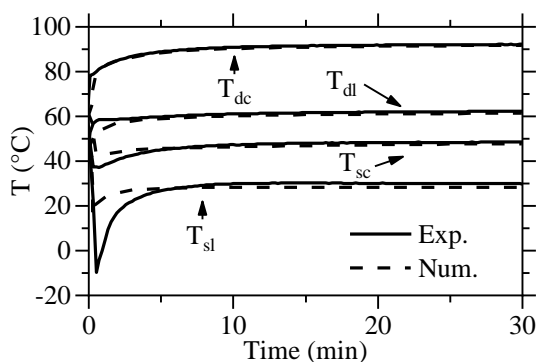

Figure 12: Numerical vs. experimental temperatures along the refrigerant path in the compressor
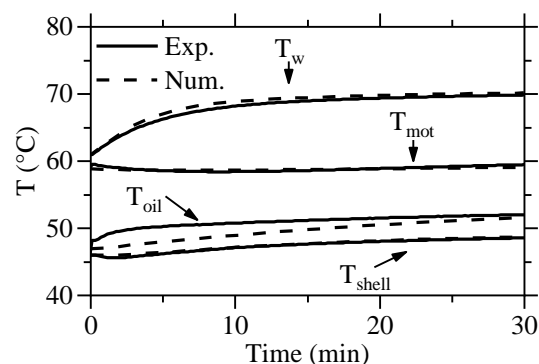

Figure 13: Numerical vs. experimental temperatures of compressor components and oil

Table 2 summarizes the deviation between experimental and numerical results for the runtime ratio (RTR) and overall energy consumption (OEC) considering four test conditions. It is worth of note that the empirical parameters were maintained fixed for all operating conditions. Despite the differences noticed during the early stages after the compressor start-up, one can see that the system simulation model is be able to predict the overall performance parameters of the refrigerator with good accuracy.

Table 2: Deviances between numerical and experimental results

T_{amb} (°C)	T_{off} (°C)	RTR Error (%)	OEC Error (%)
32	-16	-1,1	-1,4
25	-10	+0,3	+0,5
25	-19	-5,6	+6,1
16	-16	+1,4	-1,4

Figures 14 and 15 illustrate the impact of two design modifications on the compressor performance under calorimeter conditions (COP) and overall energy consumption of the refrigeration system. The calorimeter condition, Cal[CheckPoint], is given by $T_e = -23.3$ °C, $T_c = 54.4$ °C, $T_{sl} = 32$ °C and $T_{amb} = 32$ °C. The effect of a compressor design change on the COP under calorimeter conditions is compared to a baseline and presented in the primary axis. On the other hand, the variation of the refrigerator energy consumption due to compressor design change is compared to a baseline and presented in the secondary axis. Negative values of $\Delta \dot{E}$ are presented in both figures to facilitate the comparison with ΔCOP.

Figure 14 evaluates the impact of insulating the compressor suction system. As can be seen, by reducing the thermal conductance UA_{ie-sm} from its reference value to a figure close to zero, the COP under calorimeter conditions is increased between 2 and 3%, since the thermodynamic losses due to suction superheating are reduced. It can also be observed that the reduction in the overall energy consumption is lower under system conditions (~1.5%) than the increase in COP under calorimeter conditions (~2.5%). In fact, the increase of mass flow rate due to suction thermal insulation reduces the evaporating pressure, but with a consequent increase of temperature difference on the air side of the evaporator, thus increasing the external irreversibilities of the cycle. Figure 15 presents a similar analysis but focused on the compressor electrical efficiency. The results reveal that the increase in the electrical efficiency reduces the refrigerator energy consumption in a level very similar to the increase of COP measured under calorimeter conditions. This is because an increase in compressor electrical efficiency does not change significantly the mass flow rate provided by the compressor, only affecting its power consumption. It becomes clear that the benefit of a more efficient compressor in a household refrigerator is related to the type of design change that caused the COP to increase under calorimeter conditions.
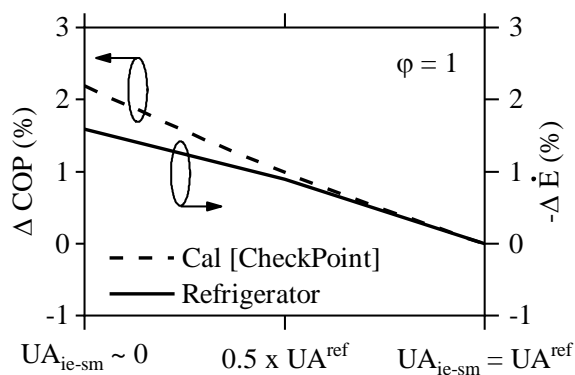

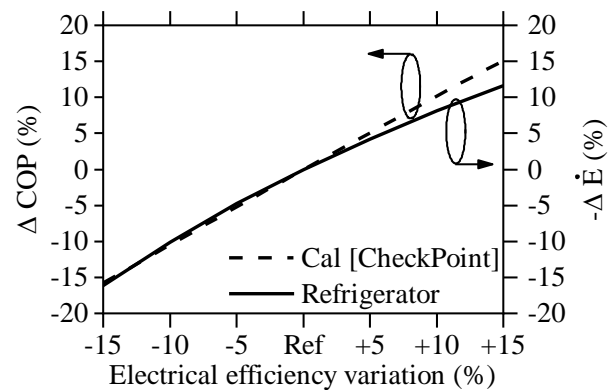**Figure 14:** Impact of suction insulation on the compressor and system performances under different working conditions

Figure 15: Impact of electrical efficiency on the compressor and system performances under different working conditions

5. CONCLUSIONS

This paper presented a novel simulation model to predict the performance of reciprocating compressors of household refrigerators operating under on-off cycling conditions. The model was focused on the compressor and, therefore, simplified approaches were used for the remaining components, while in-house experimental data was used to derive the empirical parameters required for the model closure. The model predictions were validated via comparisons with experimental data, showing differences of 1% for power consumption, 3% for mass flow rate, and maximum deviations of 6% for the runtime ratio and overall energy consumption. After being validated, the model was employed to investigate the effect of compressor design modifications on the COP estimated under calorimeter conditions and on the overall energy consumption of the refrigerator. The results reveal that the benefit of a more efficient compressor in a household refrigerator depends on the nature of the design modification that increases the COP under calorimeter conditions. This endorses the idea that actual system conditions should be considered in the compressor selection to effectively reduce energy consumption of household refrigerators.

NOMENCLATURE

h	Enthalpy	[J/kgK]	$\dot{Q}_{ele}$	Electrical losses	[W]
m	Mass	[kg]	$\dot{Q}_{pc}$	Piston-cylinder gap dissipation	[W]
$\dot{m}$	Mass flow rate	[kg/s]	T	Temperature	[ºC]
p	Pressure	[Pa]	UA	Heat conductance	[W/K]
$\dot{Q}_b$	Heat dissipation at the bearings	[W]	W_{ind}	Indicated power	[W]

Subscripts

amb	External environment		ie	Compressor internal environment
b	Related to backflow		l	Leakage
c	Condensing		mot	Electrical motor
cd	Condenser wall		oil	Lubricant oil
dis	Discharge vale orifice		pc	Piston cylinder gap
dc	Discharge chamber		rc	Refrigerated compartment
dl	Discharge line		suc	Suction valve orifice
dm	Discharge muffler		sc	Suction chamber
do	Discharge muffler outlet		se	Suction muffler inlet
dt	Discharge tube		$shell$	Compressor shell
dv	Discharge valve		sl	Suction line
e	Evaporating		sm	Suction muffler
ev	Evaporator wall		w	Compression chamber wall

REFERENCES

Annand, W. J. D. (1963). Heat transfer in the cylinders of reciprocating internal combustion engines. *Proc. I. Mech. Eng. 117 973-96.*

Barther, C. and Götz, T. (2012). *The overall worldwide saving potential from domestic refrigerators and freezers.* Wuppertal, Germany. Wuppertal Institute for Climate, Environment and Energy.

Belman-Flores, J. M., Barroso-Maldonado, J. M., Rodríguez-Muñoz, A. P., & Camacho-Vázquez, G. (2015). Enhancements in domestic refrigeration, approaching a sustainable refrigerator – A review. *Renew. Sust. Energ. Rev.*, 51, 955-968.

Borges B. N., Melo C., Hermes C. J. L. (2015) Transient simulation of a two-door frost-free refrigerator subjected to periodic door opening and evaporator frosting, *Appl. Energy*, 147, 386-395

Borges, B. N., Hermes, C. J. L., Gonçalves, J. M. & Melo, C. (2011) Transient simulation of household refrigerators: A semi-empirical quasi-steady approach. *Appl. Energy*, 88, 748–754.

Chen, Z.-j., Lin, W.-h (1991). Dynamic simulation and optimal matching of a small-scale refrigeration system. *Int. J. Refrig.*, 14, 329-335.

Deschamps, C. J., Possamai, F. C., & Pereira, E. L. L. (2002). Numerical Simulation Of Pulsating Flow In Suction Mufflers. *In: Proc. Int. Compressor Engineering Conference*, (paper 1542). West Lafayette, USA.

Diniz, M. C. & Deschamps, C. J. (2016). Performance Analysis of a Reciprocating Compressor under Typical Transients of Refrigeration Systems. *In: Proc. Int. Compressor Engineering Conference*, (paper 2448). West Lafayette, USA.

Diniz, M. C., Melo, C. & Deschamps, C. J. (2018). Experimental Performance Assessment of a Hermetic Reciprocating Compressor Operating in a Household Refrigerator under On-Off Cycling Conditions. *Int. J. Refrig,* 88, 587-598.

Ferreira, R. T. S. & Lilie, D. E. B. (1984). Evaluation of the leakage through the clearance between piston and cylinder in hermetic compressor. *In: Proc. Int. Compressor Engineering Conference at Purdue University*, (paper 424). West Lafayette, USA.

Heimel, M., Berger, E., Posch, S., Stupnik A., Hopfgartner, J. & Almbauer R (2016) Transient cycle simulation of domestic appliances and experimental validation, *Int. J. Refrig.*, 69, 28-41

Hermes, C. J. L. & Melo, C. (2008). A first-principles simulation model for the start-up and cycling transients of household refrigerators. *Int. J. Refrig.*, 31, 1341-1357.

Lemmon, E.W., Huber, M.L. & McLinden, M.O. (2002). NIST Standard Reference Database 23: Reference Fluid Thermodynamic and Transport Properties-REFPROP,Version 7.0.

Ndiaye, D. & Bernier, M. (2010). Dynamic model of a hermetic reciprocating compressor in on–off cycling operation (Abbreviation: Compressor dynamic model). *Appl. Therm. Eng.*, 30, 792-799.

Negrão, C. O. R., Erthal, R. H., Andrade, D. E. V. & Silva, L. W. (2011). A semi-empirical model for the unsteady-state simulation of reciprocating compressors for household refrigeration applications. *Appl. Therm. Eng.*, 31, 1114-1124.

Tagliafico, L. A., Scarpa, F., Tagliafico, G. (2012). A compact dynamic model for household vapor compression refrigeration systems. *Appl. Therm. Eng.*, 35, 1–8.

Todescat, M. L., Fagotti, F., Prata, A. T. & Ferreira, R. T. S. (1992). Thermal energy analysis in reciprocating hermetic compressors. *In: Proc. Int. Compressor Engineering Conference at Purdue University*, (paper 936). West Lafayette, USA

ACKNOWLEDGEMENT